2.13 Closed upstream basins with forcing and dissipation.

The cornerstone models of rotating hydraulics make the assumption that the upstream reservoir is infinite in extent and that potential vorticity q^* is conserved. In reality, oceanic basins such as the Norwegian Sea, the Greenland Sea, and the Brazil Basin are finite and are subject to forcing and dissipation. Although the deep circulations in these regions have not been mapped out, the conventional view is that the flows are weak and in near geostrophic balance. Forcing and dissipation may be weak in a local sense, but they have a cumulative effect that can be significant over the broad expanse of the basin. These processes are instrumental in the determination of q^* and it is quite unlikely that this quantity will be uniform. In fact, direct observations of the velocity of the deep flow in the Faroe-Bank Channel (Lake et al., 2005) suggest that q^* can be significantly non-uniform.

The main difficulty in trying to extend models like Gill's is one of tractability: the combination of forcing, dissipation and nonlinearity gives rise to formidable mathematical obstacles. However, one might expect nonlinear advection to be relatively unimportant in the upstream basin, where the flow is weak. In addition, one might expect forcing and dissipation to be of minor consequence within the strait that drains the basin, where advection is quite strong. The neglect of friction may not be supportable within the 'plume' region, downstream of the sill, where the relatively swift outflow descends into the downstream basin, but it may be valid upstream of the sill.

a. Linear model for the basin.

Keeping these expectations in mind, we now develop an approach in which the slow, linear, dissipative circulation in an upstream basin is linked to an inertial outflow that takes place through a strait (Figure 2.13.1). The approach is presented in greater detail by Pratt and Llewellyn Smith (1997) and Pratt (1997). The basin topography is variable and the upstream flow may be fed by a variety of sources, including deep convection, lateral inflows through other straits, or dense fluid sliding down the continental slope. Since there is no reason to expect the basin flow to take place in a preset direction, one must abandon the semi-geostrophic approximation and consider the full steady shallow water equations:

$$(\mathbf{u}^*\cdot\nabla^*)\mathbf{u}^* + f\mathbf{k}\times\mathbf{u}^* = -g\nabla^*\eta^* - \frac{r_f\mathbf{u}^*}{d^*}, \qquad (2.13.1)$$

and

$$\nabla^*\cdot(\mathbf{u}^* d^*) = w_e^*. \qquad (2.13.2)$$

where w_e* is a positive downwards entrainment velocity and r_f a drag coefficient. The elevation η* of the interface is measured relative to the sill and the depth of basin below the sill is given by d_o*:

$$d^*(x^*,y^*,t^*) = d_o^*(x^*,y^*) + \eta^*(x^*,y^*,t^*).$$

Note that the effects of entrainment have been included in the continuity equation but not the momentum equation, an approximation that the reader can justify by working through Exercise 1.

Let N and D be scales for η* and d_o* and assume that $\varepsilon = N/D << 1$. Then if $(gD)^{1/2}/f$ is a typical length scale for the basin flow, the geostrophic relation suggests $\varepsilon(gD)^{1/2}$ as a velocity scale. The corresponding nondimensional versions of (2.13.1) and (2.13.2) are given by

$$\varepsilon(\mathbf{u}\cdot\nabla)\mathbf{u} + \mathbf{k}\times\mathbf{u} = -\nabla\eta - \frac{r_f\mathbf{u}}{fD(d_o+\varepsilon\eta)}, \tag{2.13.3}$$

and

$$\nabla\cdot[\mathbf{u}(d_o+\varepsilon\eta)] = \frac{w_e^*}{fN}, \tag{2.13.4}$$

where $D(x,y)$ is the nondimensional basin depth below sill level.[1] It is assumed that friction and entrainment are weak and this is formalized by replacing r_f/fD and w_e^*/fN with εR_f and εw_e, where the nondimensional functions R_f and w_e are regarded as O(1).

The next step is to expand the dependent variables in power series in ε:

$$\mathbf{u} = \mathbf{u}^{(0)} + \varepsilon\mathbf{u}^{(1)} + \cdots \tag{2.13.5}$$

and

$$\eta = \eta^{(0)} + \varepsilon\eta^{(1)} + \cdots. \tag{2.13.6}$$

The lowest order approximations to (2.13.3) and (2.13.4) are just the geostrophic relation $\mathbf{k}\times\mathbf{u}^{(0)} = -\nabla n^{(0)}$ and $\nabla\cdot(\mathbf{u}^{(0)}d_o) = \mathbf{u}^{(0)}\cdot\nabla d_o = 0$, which show that fluid circulates along contours of constant D. At the present order of approximation, these 'geostrophic' contours are equivalent to contours of constant f/d*.

In order to determine the strength of the circulation on a particular contour, it is necessary to proceed to the next order of approximation:

[1] Not to be confused with the usage elsewhere of D as a depth scale.

$$\mathbf{k}\times\mathbf{u}^{(1)}+\nabla\eta^{(1)}=-(\mathbf{u}^{(0)}\cdot\nabla)\mathbf{u}^{(0)}-\frac{R_f\mathbf{u}^{(0)}}{d_o} \qquad (2.13.7)$$

and

$$\nabla\cdot[\mathbf{u}^{(1)}d_o]=-\nabla\cdot[\mathbf{u}^{(0)}\eta^{(0)}]-w_e \qquad (2.13.8)$$

Now consider a closed geostrophic contour C having unit normal and tangent vectors $\boldsymbol{n}$ and $\boldsymbol{l}$ and arclength coordinate s (Figure 2.13.1a). Integration of the tangential component of (2.13.7) about C and use of $\boldsymbol{u}^{(0)}\cdot\mathbf{n}=0$ leads to

$$d_o\oint_C\mathbf{u}^{(1)}\cdot\mathbf{n}ds=-R_f\oint_C\mathbf{u}^{(0)}\cdot\mathbf{l}ds\,. \qquad (2.13.9)$$

Integration of (2.13.8) over the area A_C enclosed in C gives

$$d_o\oint_C\mathbf{u}^{(1)}\cdot\mathbf{n}ds=\iint_{A_C}w_e d\sigma\,. \qquad (2.13.10)$$

Equation (2.13.9) is a form of Kelvin's theorem stating that the damping of circulation $\oint_C\mathbf{u}^{(0)}\cdot\mathbf{l}ds$ due to bottom friction is balanced by the input of circulation as the result of advection of planetary vorticity f (nondimensionally unity) across the contour by the normal velocity $\mathbf{u}^{(1)}\cdot\mathbf{n}$. Equation (2.13.10) relates this normal velocity to the influx of volume by the entrainment velocity acting over the area enclosed by the contour. Had our formulation taken the bottom Ekman layer into consideration, the cross contour flow would have been confined to this layer. In the present slab model, the velocity is evenly distributed over the layer depth.

Subtraction of the last two equations gives an expression for the average geostrophic speed about the contour

$$\oint_C\mathbf{u}^{(0)}\cdot\mathbf{l}ds=-R_f^{-1}\iint_{A_C}w_e d\sigma\,. \qquad (2.13.11)$$

The reader may wonder how the above steps were discovered. The roots of the procedure for obtaining (2.13.11) can be found in Greenspan (1990). Our asymptotic expansion yields a lowest order approximation (the geostrophic flow) that cannot be completely determined. The standard resolution to this problem of 'geostrophic degeneracy' is that one proceeds to the next order of approximation. In order to calculate the O(ε) fields a solvability condition must first be satisfied and it is this condition that determines the geostrophic fields. In quasigeostrophic theory (e.g. Pedlosky 1987) the compatibility condition is the quasigeostrophic potential vorticity equation obtained from the O(ε) equalities. Our problem differs from quasigeostrophic dynamics only by the allowance for large depth variations; the compatibility condition (2.13.11) is the same as that obtained by integrating the potential vorticity equation over the area enclosed in a

geostrophic contour (see Exercise 2). Our use of the circulation integral is simply a shortcut to this procedure.

Consider an isolated patch of downwelling (Figure 2.13.1a) that is bisected by C. Equation (2.13.11) dictates that the average geostrophic velocity about C is proportional to the volume flux due to downwelling over the portion of the patch lying inside C. The geostrophic interface elevation $\eta^{(0)}$ is constant along C and its value can be determined from the relation $\mathbf{u}^{(0)} \cdot \mathbf{l} = \partial \eta^{(0)} / \partial n$. Let α be a parameter that identifies the contour (C=$C(\alpha)$). Then

$$\mathbf{u}^{(0)} \cdot \mathbf{l} = \frac{d\eta^{(0)}}{d\alpha} \frac{\partial \alpha}{\alpha n}, \tag{2.13.12}$$

and (2.13.11) becomes

$$\frac{d\eta^{(0)}}{d\alpha} \oint_C \frac{\partial \alpha}{\partial n} ds = -R_f^{-1} \iint_{A_C} w_e d\sigma . \tag{2.13.13}$$

Since $\partial \alpha / \partial n$ is given by the geometry of the geostrophic contours, its integral can be determined as a function of α, as can the right-hand side of (2.13.13). The result is a first-order differential equation for $\eta^{(0)}$. Once the solution is obtained the value of geostrophic velocity at any point in the basin can be calculated from (2.13.12).

As an example, consider a basin with azimuthal symmetry (Figure 2.13.2). All of the constant d_o contours are circular and the flow is fed by a central, uniform patch of downwelling:

$$w_e = \begin{cases} T / \pi r_o^2 & (r < r_o) \\ 0 & (r \geq r_o) \end{cases}. \tag{2.13.14}$$

The resulting geostrophic flow circulates around the circular geostrophic contours. Let u and v temporarily denote the radial and azimuthal velocity components, so that $u^{(0)}$=0 and (2.13.11) gives

$$v^{(0)} = \frac{-T}{2\pi r R_f} \begin{cases} r^2 / r_o^2 & (r < r_o) \\ 1 & (r \geq r_o) \end{cases}. \tag{2.13.15}$$

The geostrophic relation $v^{(0)} = \partial \eta^{(0)} / \partial r$ can then be integrated to obtain the interface elevation

$$\eta^{(0)} = \eta^{(0)}(a) - \frac{T}{2\pi r R_f}\begin{cases} \ln(r_o / a) + (r^2 - r_o^2)/2r_o^2 & (r < r_o) \\ \ln(r_o / a) & (r \geq r_o) \end{cases}, \qquad (2.13.16)$$

where a is the basin radius. Finally, the radial velocity is determined from (2.13.10) as

$$u^{(1)} = \frac{T}{d_o(r)2\pi r}\begin{cases} r^2 / r_o^2 & (r < r_o) \\ 1 & (r \geq r_o) \end{cases}. \qquad (2.13.17)$$

In summary, specification of the transport T yields a basin circulation determined to within a constant, with no regard for boundary conditions or interactions with the strait and sill. The constant is $\eta^{(0)}(a)$, the interface elevation above the sill at the basin edge $r=a$. The leading order radial and azimuthal velocities are completely determined. If the basin is closed except for a single draining channel, then the normal component of the transport velocity $\mathbf{u}^{(1)}d_o$ must be zero at solid edges and must take on some finite distribution (yet to be determined) at the channel entrance. On the other hand, the flow might fed by dense fluid sliding down the sloping walls of the basin or by inflow from a second strait. Then the correct boundary condition may involve the specification of the normal component of $\mathbf{u}d$ about the perimeter. Evaluation of (2.13.17) at the basin edge $r=a$ leads $u^{(1)}(a)d_o(a) = T / 2\pi a$, which generally satisfies neither of these conditions.

(b) Diffusive boundary layer.

A boundary layer is clearly needed to close the circulation and we therefore append (2.13.5) and (2.13.6) so as to include boundary layer fields $\tilde{u}$, $\tilde{v}$, and $\tilde{\eta}$ that decay inwards from the edges of the basin:

$$u = \varepsilon u^{(1)}(r) + \varepsilon\tilde{u}(\xi,\theta) + \cdots, \qquad (2.13.18)$$

$$v = v^{(0)}(r) + \varepsilon v^{(1)}(r,\theta) + (\varepsilon / \delta)\tilde{v}(\xi,\theta), \qquad (2.13.19)$$

$$\eta = \eta^{(0)}(r) + \varepsilon\eta^{(1)}(r,\theta) + \varepsilon\tilde{\eta}^{(1)}(\xi,\theta) + \cdots \qquad (2.13.20).$$

Here, δ represents the boundary layer thickness and $\xi = (a - r)/\delta$ is a stretched coordinate that varies by O(1) over this thickness . The size of the boundary layer correction $\varepsilon\tilde{u}(\xi,\theta)$ in (2.13.18) is dictated by the requirement that the O(ε) interior radial velocity must be brought to zero at $\xi=0$. The correction $(\varepsilon / \delta)\tilde{v}(\xi,\theta)$ to the azimuthal velocity in (2.13.19) is determined by the requirement that the boundary layer must drain the O(ε) radial transport and carry it to the channel entrance within an O(δ) width. Since $(\varepsilon/\delta) >> \varepsilon$, $\tilde{v}(\xi,\theta)$ enters the problem at a lower order than does dissipation, forcing and nonlinearity; hence this velocity will be geostrophically balanced . The normal derivative

$\partial / \partial r = \delta^{-1} \partial / \partial \xi$ of the boundary layer correction for η must therefore be O(ε/δ) , and the correction must itself be O(ε), as specified in (2.13.20).

The dynamics of the boundary layer can be determined through substitution of (2.13.18-20) into (2.13.3) and (2.13.4) and identification of the largest terms involving boundary layer fields. The thickness δ is then chosen in order to achieve a balance between these terms. This procedure is detailed in Pratt (1997), who finds that $\delta=\varepsilon^{1/2}$ and that the boundary layer is governed by:

$$\tilde{u}\left[\frac{\partial D}{\partial r}\right]_{r=a} + \frac{\tilde{v} D(a)}{a} \frac{\partial^2 \tilde{v}}{\partial \theta \partial \xi} + R_f \frac{\partial \tilde{v}}{\partial \xi} = 0 \,. \qquad (2.13.21)$$

The dynamical balance is one between various sources and sinks of vorticity. As a fluid column enters the boundary layer from the interior and moves up the sloping bottom towards the wall, negative vorticity is generated as a result of squashing of the column (first term). This effect is balanced by advection of vorticity along the wall (middle term) and diffusion of vorticity into the wall (final term). If the wall depth $d_o(a)$ is zero, or at least <<1, the middle term may be neglected. Under this condition, use of the geostrophic balance

$$\tilde{v} = -\frac{\partial \tilde{\eta}}{\partial \xi} \text{ and } \tilde{u} = -\frac{1}{a} \frac{\partial \tilde{\eta}}{\partial \theta}$$

leads to a single equation for the normal boundary layer velocity:

$$\alpha^2 \frac{\partial \tilde{u}}{\partial \theta} - \frac{\partial^2 \tilde{u}}{\partial \xi^2} = 0 \,, \qquad (2.13.22)$$

where $\alpha^2 = \dfrac{-[d(d_o)/dr]_{r=a}}{a R_f}$.

Equation (2.13.22) is a diffusion equation with the time variable replaced by θ. The corresponding boundary layer on a straight coast is sometimes referred to as the "arrested topographic wave" (Csanady 1978). The solution is also equivalent to the northern or southern boundary layer arising in a homogeneous Stommel circulation on a β-plane (Pedlosky, 1968). In the present setting, the sloping boundary at the basin edge provides a topographic β effect that makes the edge act like a Stommel northern boundary, with increasing θ equivalent to the westward direction.

(c) Joining the basin to the strait.

In order to pose boundary conditions on (2.13.22) it is necessary to consider the conditions in the strait. In general, the fluid from outside has non-uniform potential

vorticity and will have a complicated velocity distribution as it enters the strait. If this flow is hydraulically controlled at some point in the interior of the channel, it may be possible to relate the volume flux T to the interface elevation at the entrance by a weir relation. Although no general relation is available under conditions of non-uniform potential vorticity, the situation becomes considerably simplified if the layer thickness d over the sill is relatively small compared to d in the entrance region (Figure 2.13.1a). Fluid columns entering the strait must therefore be severely squashed as they pass over the sill, rendering $\partial v / \partial x \cong -f$, as assumed in the WLK model (Section 2.4). We will also assume that the strait width is much less than the nominal deformation radius (dimensionally $w_s^* << (gD)^{1/2} / f$), so that the variation in η over the width is <<1. Under these conditions, the assumptions of the WLK theory hold provided that Δz^* in the weir formula [(2.4.10) is for attached sill flow or (2.4.15) for separated sill flow] is equated with interface elevation η_e^* at the entrance to the strait, and not in the interior of the basin. If the basin source transport T^* is matched to the transport Q^* given by these formulae, and the various scaling factors are reconciled, one obtains

$$T = \begin{cases} \left(\frac{2}{3}\right)^{3/2} w_s \left[\eta_e - \frac{w_s^{\,2}}{8}\right]^{3/2} & (w_s^{\,2} < 2\eta_e) \\ \eta_e^{\,2} / 2 & (w_s^{\,2} \geq 2\eta_e) \end{cases}, \qquad (2.1.23)$$

where $w_s = w_s^* f / (gN)^{1/2}$. The strait width w_s^* scales with the deformation radius based on N, while the basin scale is generally assumed be $\geq$ the deformation scale based on D ($>>N$). Since $\varepsilon = N/D$, the strait occupies a vanishingly small portion of the basin circumference as $\varepsilon \to 0$.

Returning to the question of boundary conditions, the value of u must be zero along the basin edge: $u(a,\theta) = \varepsilon(u^{(1)}(a) + \tilde{u}(0,\theta)) = 0$ for values of θ away from the entrance. Suppose that the entrance is centered at θ=0 and that the basin edge spans $-\pi \leq \theta < \pi$. As $\varepsilon \to 0$, the strait exists only within a vanishingly small interval about θ=0. The boundary condition there must be chosen to insure that the correct transport is accommodated. Thus

$$\tilde{u}(0,\theta) = -u^{(1)}(a) + \frac{T\delta(\theta)}{aD(a)} \qquad (2.13.24)$$

where $u^{(1)}(a) = T / 2\pi a d_o(a)$ and where $\delta(\theta)$ denotes the Dirac delta function. Note that the integral of $u(a,\theta)$ across the strait entrance gives the correct transport:

$$\lim_{\theta_o \to \infty} \int_{-\theta_o}^{\theta_o} d_o(a) u^{(1)}(a,\theta) a d\theta = T \int_{-\theta_o}^{\theta_o} \delta(\theta) d\theta = T \, .$$

A general solution to (2.13.22) for the periodic geometry is

$$\tilde{u} = \mathrm{Re}\left\{ \sum_{i=0}^{n} A_n U_n(\xi) e^{in\theta} \right\}, \tag{2.13.25}$$

with $U_n(\xi) = e^{-\alpha(1+i)(n/2)^{1/2}\xi}$. Application of the boundary condition (2.13.24) leads to

$$A_o = -u^{(1)}(a) + \frac{T}{2\pi a d_o(a)} = 0 \text{ and } A_n = \frac{T}{\pi a d_o(a)} \ (n \geq 1). \tag{2.13.26}$$

One of the weaknesses of the above solution is that it does not resolve the flow near the entrance of the strait. The boundary layer approximation is lost within an $\varepsilon^{1/2} \times \varepsilon^{1/2}$ entrance region where the flow must turn the corner and enter the strait. Also, the depth $d_o(a)$ across the entrance has tacitly been assumed to match the constant depth about the perimeter of the basin, an assumption that leads to problems when $d_o(a)$ vanishes. In such cases, $d_o(a)$ needs to be replaced by the actual strait depth.

To close the problem completely, it only remains to evaluate the integration constant $\eta^{(o)}(a)$ in (2.13.16). Since the interface elevation changes by only $O(\varepsilon)$ across the boundary layer, and by extension, the $\varepsilon^{1/2} \times \varepsilon^{1/2}$ entrance region, we may approximate the elevation η_e just inside the entrance by $\eta^{(o)}(a)$. Equation (2.13.23) can then be inverted to obtain

$$\eta^{(o)}(a) = \begin{cases} \dfrac{3}{2}\left(\dfrac{T}{w_s}\right)^{2/3} + \dfrac{{w_s}^2}{8} & ({w_s}^2 < 2\eta_e) \\ (2T)^{1/2} & ({w_s}^2 \geq 2\eta_e) \end{cases}. \tag{2.13.27}$$

The complete solution for the basin is now given by (2.13.15-17) and (2.13.27). The horizontal circulation can be summarized by considering an element of fluid introduced into the middle of the basin as a result of the downwelling. The element circulates anticyclonically and slowly spirals outwards until it reaches the basin edge, where it enters the boundary layer. The contribution to the azimuthal velocity from the boundary layer is weak in comparison to the O(0) azimuthal velocity, and the element therefore continues to circulate anticyclonically in the boundary layer. The main impact of the boundary layer will be to allow the element to pass into the strait.

Since the total transport T out of the basin is specified, the effect of the sill is contained entirely in $\eta^{(0)}(a)$. If T changes, $\eta^{(0)}(a)$ is altered according to (2.13.27) and the interface elevation at the edge of the basin is raised or lowered. The overall circulation intensifies or diminishes uniformly and the interface in the basin becomes more or less domed [see (2.13.15) and (2.13.17)]. The circulation pattern is not altered, however. In a more realistic model, the downwelling velocity w_e might itself be altered by changes in the interface elevation and this would allow the circulation pattern to change.

If the fluid is introduced into the basin laterally, with w_e=0 over the interior, then there is no interior circulation and the source water is transported entirely in boundary layers. Suppose that the basin is fed by an inflow at the opposite edge of the basin ($\theta=\pi$) from the draining strait. Then the boundary condition (2.13.24) is replaced by

$$\tilde{u}(0,\theta) = \frac{T}{ad_o(a)}(\delta(\theta) - \delta(\theta - \pi)),$$

and the coefficients in (2.13.25) become

$$A_0 = 0 \quad \text{and} \quad A_n = \frac{2T}{a\pi D(a)}. \tag{2.13.28}$$

The inflow splits into two boundary layers that circle the basin and join at the draining strait (Figure 2.13.3). Note the overshoot of the cyclonic boundary layer, which causes the bulk of the flow to enter the strait along the 'left' wall of the basin.

A striking difference between the flows driven by downwelling and those driven by injection through the side walls lies in the way the fluid approaches the draining strait. In the first case the flow about the outer rim of the basin is anticyclonic and all the fluid approaches along the 'left' wall (facing into the draining strait). In the second case, the rim flow is split into two boundary layers carrying equal transports and the approach is from both walls (discounting the overshooting effect that diverts more fluid to the left wall immediately upstream of the exit). Some insight into the dynamical processes responsible for these differences can be gained by developing a circulation theorem for the rim flow. To this end, consider the shallow water momentum equations in the vector form (2.1.15). If the tangential component of this equation is integrated about a circuit C_R that follows the basin perimeter and cuts across the entrance to any straits, one obtains

$$\frac{\partial}{\partial t^*}\oint_{C_R} \mathbf{u}^* \cdot \mathbf{l} ds = -\oint_{C_R} (\zeta^* + f)\mathbf{u}^* \cdot \mathbf{n} ds + \oint_{C_R} \mathbf{F}^* \cdot \mathbf{l} ds, \tag{2.13.29}$$

where the integration direction is counterclockwise. The rate of change of circulation $\oint_{C_R} \mathbf{u}^* \cdot \mathbf{l} ds$, essentially the net swirl velocity about rim, is therefore equal to the flux of absolute vorticity $\zeta^* + f$ across the rim (due to inflows and outflows) plus the tangential component of forcing and dissipation along the rim.

In the cases considered above $\partial / \partial t^* = 0$, $\mathbf{F}^*$=-$r_f\mathbf{u}^*/d^*$, and $\zeta^* << f$. With a downwelling-driven flow drained by a single strait, (2.13.29) reduces to

$$r_f \oint_{C_R} \frac{\mathbf{u}^* \cdot \mathbf{l}}{d^*(a)} ds = -f \oint_{C_R} \mathbf{u}^* \cdot \mathbf{n} ds = -fT^*/d^*(a) < 0,$$

and therefore the net swirl velocity about the rim must be negative, as observed. For the case in which fluid is introduced through a source strait, we have

$$r_f \oint_{C_R} \frac{\mathbf{u}^* \cdot \mathbf{l}}{d^*(a)} ds = -fT^*/d^*(a) + fT^*/d^*(a) = 0 .$$

The net swirl velocity in this case is zero, a property consistent with the presence of boundary layers on both left and right walls.

(d) Numerical simulations and the potential vorticity of the outflow.

Numerical experiments based on the full shallow-water equations (Helfrich and Pratt 2003) have reproduced the overall circulation patterns anticipated by the linear theory. In the three simulations shown in Figure 2.13.4, fluid is introduced into a bowl shaped basin at the same volume rate but in different geographic locations. The patterns of currents that arise in the basin largely follow expectations based on basin circulation integrals. As the location of the source is changed the flow patterns become quite different. On the other hand, the draining flow in the rectangular strait is remarkably consistent from one case to the next (Figure 2.13.5).

The linear model uses a weir formula based on 'zero potential vorticity' theory, but this approximation is not enforced in the numerical simulations. The potential vorticity (q) in the strait is self determined and its value and distribution provide a basis for comparison with the cornerstone hydraulic models, most of which are based on uniform q. The observed potential vorticity distribution is non-uniform (Figure 2.13.6c), but the flow in the strait turns out to be qualitatively the same as that given by the Gill (1977) model for the same transport Q and with Gill's constant q replaced by the mean value $\overline{q}$ measured across the entrance to the strait. A comparison between two realizations (Figure 2.13.6, frames a and b vs. frames d and e) reveals only minor differences.

As suggested above, the flow in the strait, and the value of $\overline{q}$ in particular, are insensitive to the distribution of sources in the upstream basin. In fact $\overline{q}$ also tends to be quite insensitive to the value of the friction coefficient. As it turns out, the main factors controlling the potential vorticity are the sill width and the ratio of the sill elevation to the entrance elevation of the channel.[2] The potential vorticity selection can be therefore viewed as an aspect of the upstream influence due to the hydraulic control at the sill. The selection of $\overline{q}$ is clarified somewhat by consideration of the possible Gill solutions for a given strait geometry and transport Q. With Q and the sill geometry fixed, the Gill model still permits a range of steady, critically controlled solutions, each with its own q. The velocity and depth profile at the channel entrance is different in each case. An interesting quantity to focus on is the elevation Δz_R of the interface at the right wall. Helfrich and

[2] In the Helfrich and Pratt (2003) experiment, the entrance width is different than the sill width and their ration provides a third geometric parameter that influences the observed value of $\overline{q}$.

Pratt (2003) find that the observed $\overline{q}$ corresponds to a Gill solution for which Δz_R is maximized, or very nearly so, over the range of permissible solutions. Since the maximization occurs for fixed Q $[= (\Delta z_R^2 - \Delta z_L^2)/2]$, it follows that the left wall elevation Δz_L is also maximal.

In the linear model, the mean basin interface elevation is determined completely by the flux Q. If the latter is held fixed and the sill height is raised, the basin interface elevation is uniformly raised at the same rate. The same behavior is found in the numerical model, where a change in sill height simply causes the mean basin interface level to change an equal amount. Since Δz_R and Δz_L are maximal for all the possible Gill solutions with a particular Q, there is a strong suggestion, if not outright verification, that the basin has the maximum mean elevation over all such solutions. Of all the possible basin states corresponding to the various Gill solutions, the one realized apparently has maximal potential energy. The basin flow is highly subcritical, with kinetic energy dominated by potential energy, and a finding of maximal potential energy is tantamount to one of maximum energy.

e. Upstream monitoring.

We have seen that changes in the location of the source has a profound effect on the circulation and the shape of the interface in the basin, but not in the strait. Transport formulae that are based on a single measurement of the upstream interface elevation, are therefore risky to use. In fact, Gill's (1977) transport relation (Section 2.5d) fails in the present experiments when the parameter ψ_I is measured in the interior of the upstream basin. Opportunities for monitoring the flow from the entrance to the channel are more promising. The numerical solutions, which all maximize the right wall interface elevation Δz_R, tend to have relatively sluggish flow in that region (see Figure 2.13.6d or e). The Bernoulli function at this location is therefore nearly proportional to Δz_R. If it is also the case that the flow is separated at the sill, then by the arguments presented in Section 2.6, the dimensional transport is given by (2.6.7b), with the properly interpreted Δz_R*.

Even when the sill flow is not separated, the robust nature of the strait flow means that monitoring is best done using quantities measured at the strait entrance rather than in the basin proper.

f. 'Westward' intensification of the approach flow.

The presence of sluggish flow near the entrance right-wall (and rapid flow at the left wall) has also been observed in laboratory experiments by Whitehead and Salzig (2001) and is suggested by the linear theory for the basin flow (Figure 2.13.3). In the experiment (Figure 2.13.7) fluid is pumped into a deep, arc-shaped basin and it escapes through a broad, shallow channel. As a fluid column enters the channel it becomes squashed and acquires excess anticyclonic vorticity. There are two scenarios describing what happens next. In the first, which is consistent with traditional, inviscid hydraulic theory, the fluid simply continues into the channel and develops a strong shear. In the

Gill (1977) model, for example, the shear would be confined to a boundary layer. The anticyclonic would favor the left wall boundary layer, and thus the flow would enter along that wall. In the second scenario, which is consistent with ideas about slow, nearly-geostrophic flow, the flow tends to follow the isobaths, crossing them only to an extent allowed by friction. This is exactly what happens in the above linear model, where a strong swirling flow along the closed isobaths is accompanied by a weak flow towards shallower depths. The excess vorticity generated by the vortex squashing is dissipated by friction. In the entrance region, the isobaths are not closed but, instead, intersect the left and right walls of the channel. These isobaths steer fluid towards the walls, where frictional boundary layers may exist. Once a fluid column has reached a frictional boundary layer, it is able to more easily cross isobaths and continue further into the channel. The question now is whether the left- or right-wall boundary layer is preferred.

In the earlier linear model, where the isobaths parallel the basin edge, the frictional boundary layer (or 'arrested topographic wave') is different than the frictional layer that exists near the entrance, where the isobaths intersect the sidewalls. It was first established by Stommel (1948) that such a layer can occur only where the ambient potential vorticity f/ d_o^* increases in the direction with the wall on the left. For a broad ocean basin with constant depth d_o^*, and a Coriolis parameter f that increases to the north, the frictional layer must occur on the western boundary. In the present channel, where f is constant but d_o^* decreases into the strait, the boundary layer must occur on the left wall. It is expected, then, that the flow entering the strait should be concentrated along this 'dynamical western boundary', a feature bourn out by the laboratory and numerical experiments. This 'westward' intensification can also be motivated using a circulation integral, as explored in Exercise 5. The effect may account for the observation that the Denmark Strait overflow hugs the Iceland coastline, its dynamical western boundary, upstream of the sill (Jonsson and Valdimarsson, 2004). Support for this idea can also be seen in the inflow to the Barents Sea (Slagstad and McClimans, 2005).

Exercises

1. The effects of entrainment have been included in the continuity equation (2.13.2) but not in the momentum equation (2.13.1). Using results obtained in Section 1.10, show that the conditions under which this assumption is valid are $w_e/fr_f \ll 1$ and $(g'd/v^2)(w_e/r_f) \ll 1$. (The second condition is clearly more stringent than the first for the conditions in the basin.)

2. Derive the potential vorticity equation for the geostrophic flow component of the basin flow. Show that integration of this equation over the area A_C enclosed by a closed geostrophic contour yields the relation (2.13.11).

3. Suppose that some of the constant depth contours intersect the vertical side walls of the basin and are therefore not closed. How are the tangential and normal flow to the contour determined?

4. Derive equation (2.13.29) beginning with the momentum equation immediately above it.

5. (*Westward intensification of basin flow).* Consider the (northern hemisphere) case in which fluid is injected into a basin through one strait and drained through another, with no interior downwelling. Suppose that the source strait enters the north edge of the basin and the draining strait leaves the south edge. The basin is large enough for the beta effect to be important and therefore the value of f at the mouth of the source strait is larger than that at the mouth of the draining strait. Argue the flow in the basin will be concentrated in a western boundary layer. Show that the same effect occurs in an f-plane basin if the depth at the mouth of the source strait is greater than the depth at the entrance of the draining strait. Show that the same results hold for a southern hemisphere basin.

Figure Captions

2.13.1 Definition sketch.

2.13.2 Basin with azimuthal symmetry.

2.13.3 Example of solutions from the linear model in which fluid is fed into the parabolic basin through a strait in the side wall. The geometries of the entrance and exit are identical. The parameters are given by T=1, R_f=0.2, a=4.0, and w_s=0.5. (Figure 7 of Pratt, 1977)

2.13.4 Three numerical simulations of a basin flow that is drained through a strait. The fluid is introduced into the basin (a) through the back wall (at x=-15), (b) through a downwards entrainment velocity w_e distributed uniformly over the basin, and (c) through a w_e concentrated near the back wall of the basin. The contours are ones of interface elevation. (Figure 7 from Helfrich and Pratt 2003).

2.13.5 Side views of interface elevations along (a) the left wall, (b) along the centerline, and (c) along the right wall of the basin and channel for the three flows depicted in Figure 2.13.4. (Figure 6 of Helfrich and Pratt 2003).

2.13.6 Comparison of the strait flows in plan view from the numerical experiments (a-c) and the Gill (1997) theory (d-e) based on the mean potential vorticity $\overline{q} = 1.78$ measured at the entrance (dotted line). The nondimensional parameters are given in both cases by Q=.05, w_s=1, and R_f=.01. Also, the ratio of the sill elevation to the entrance elevation (both measured above the deepest point of the basin) is 0.8.

2.13.7 (a) Plan view of laboratory flow established by injecting fluid into a deep basin (left) and allowing it to drain through a shallow strait with a flat bottom (right). The width of the channel is roughly one deformation radius based on the elevation difference between the maximum surface height in the deep basin and the channel bottom. The streak lines are due to the motion of white floats. (From Whitehead and Salzig, 2001). (b) Side view showing the sloping bottom in the deep basin.

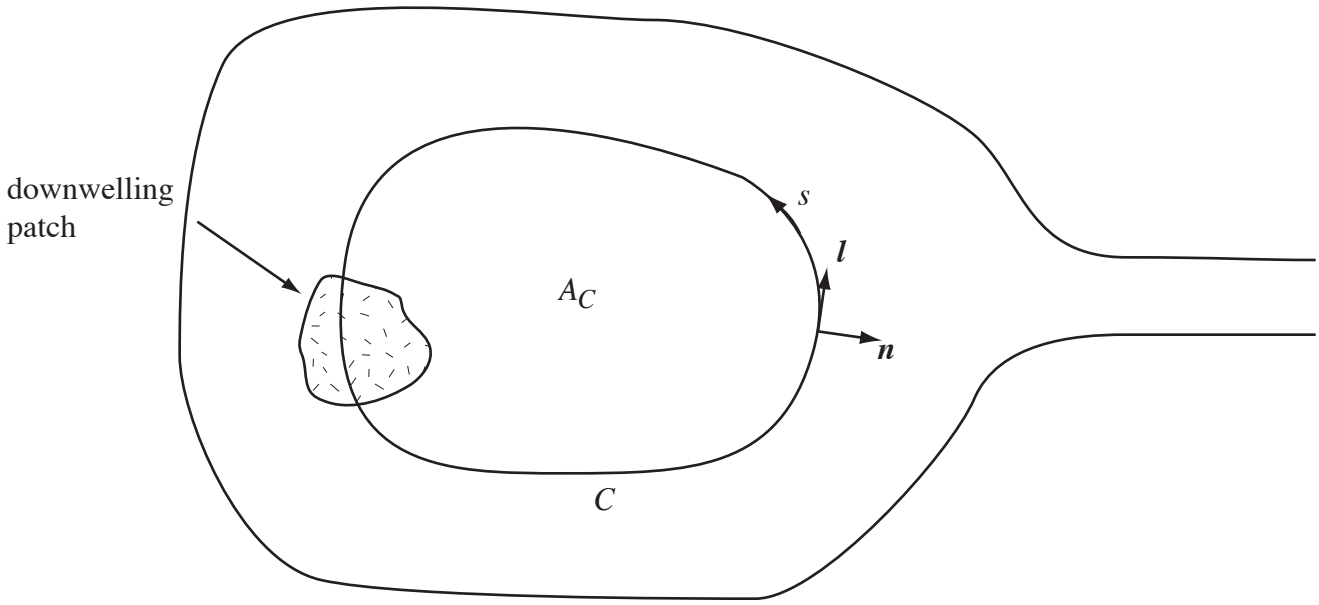

(a)

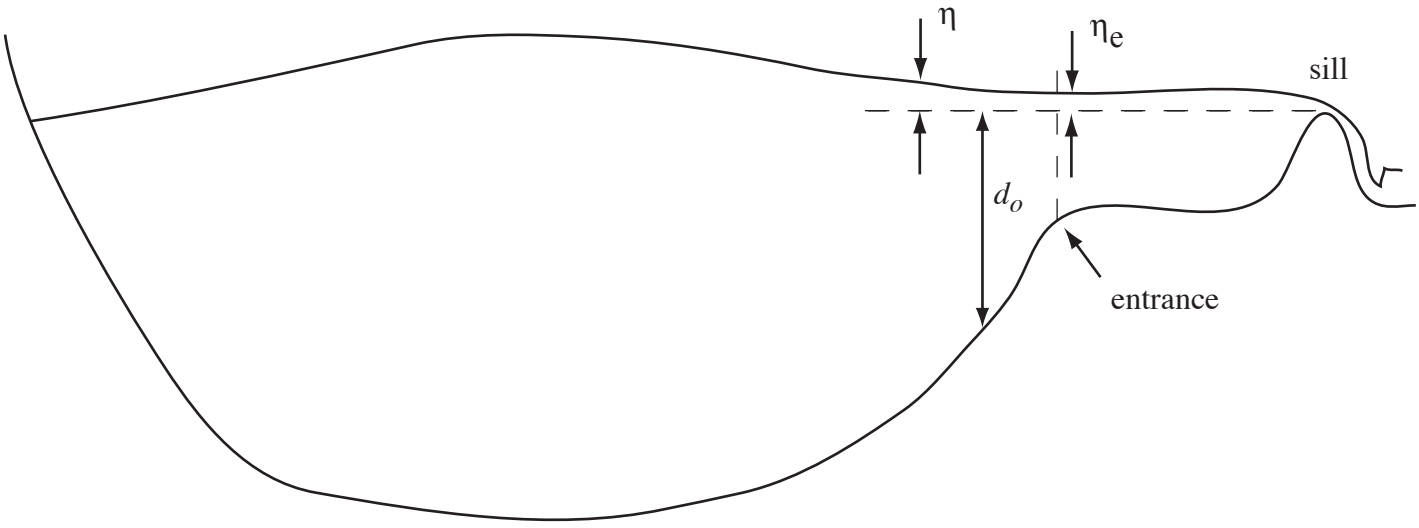

(b)

Figure 2.13.1

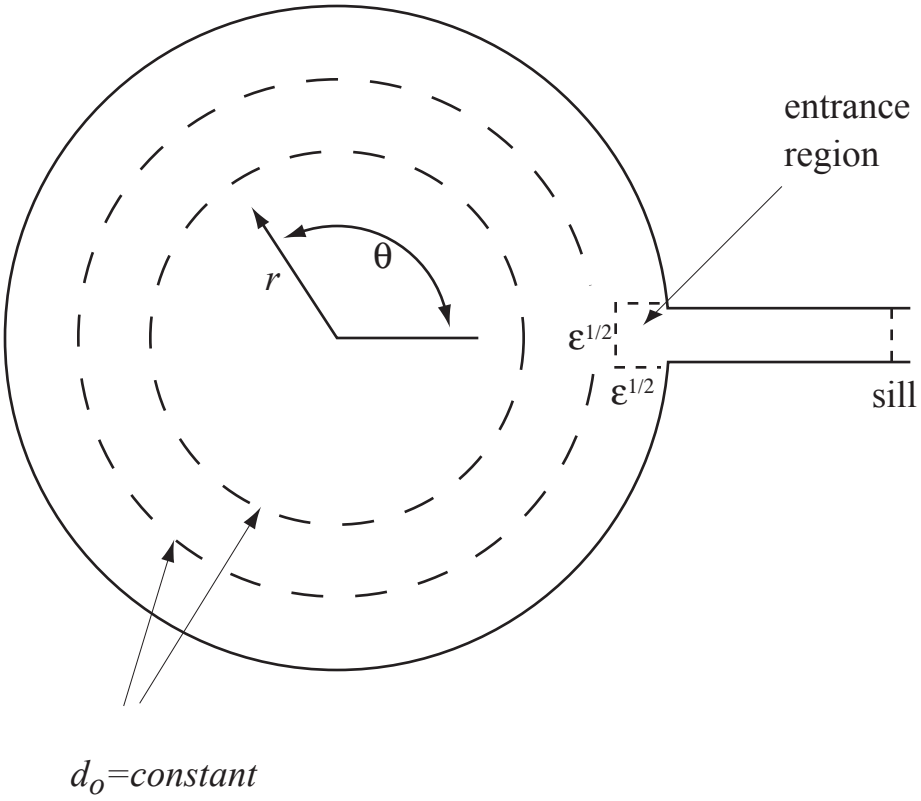

Figure 2.13.2

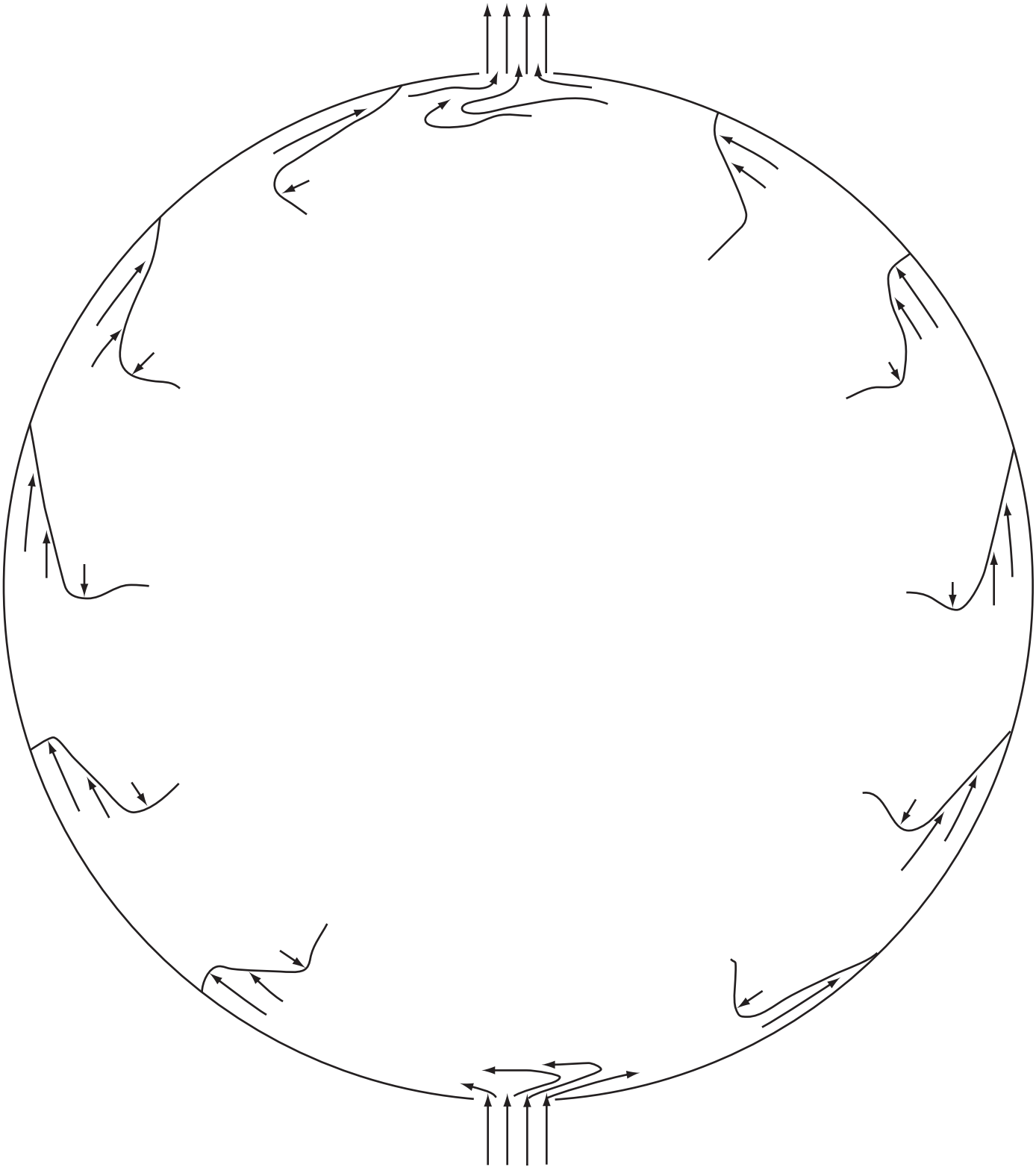

Fig 2.13.3

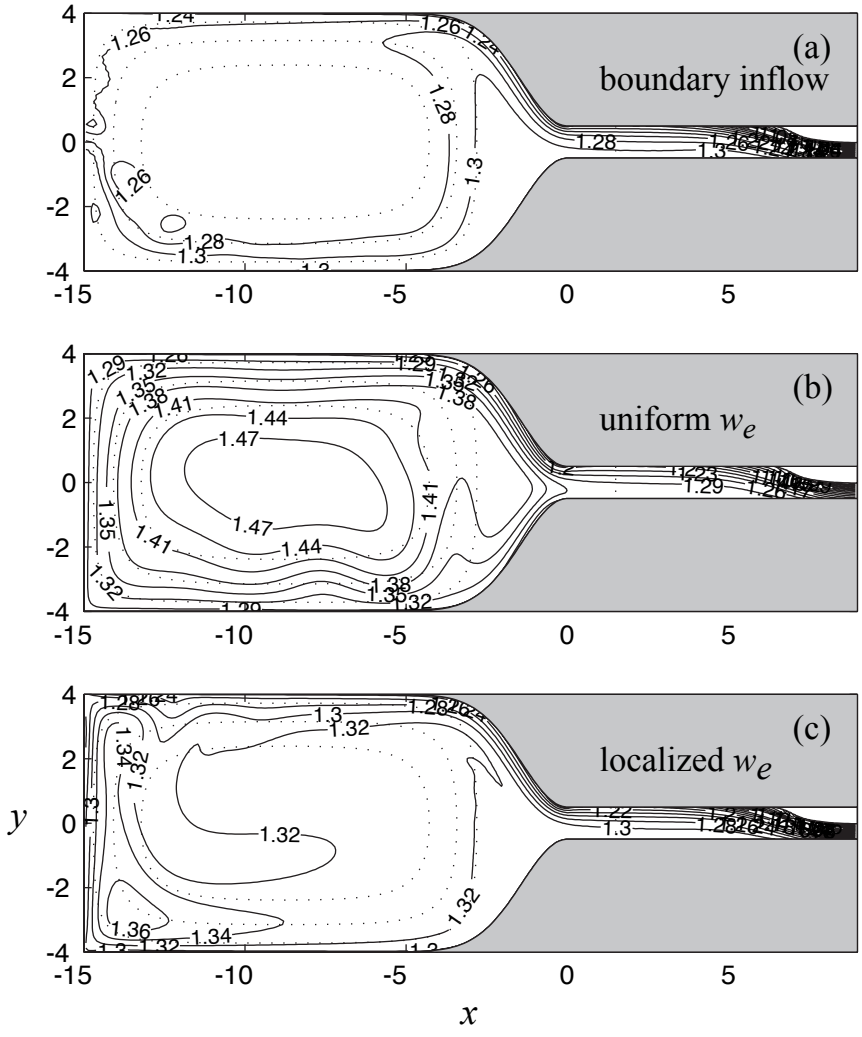
(a)
boundary inflow
(b)
uniform w_e
(c)
localized w_e
y
x
4
2
0
-2
-4
-15
-10
-5
0
5

Fig. 2.13.4

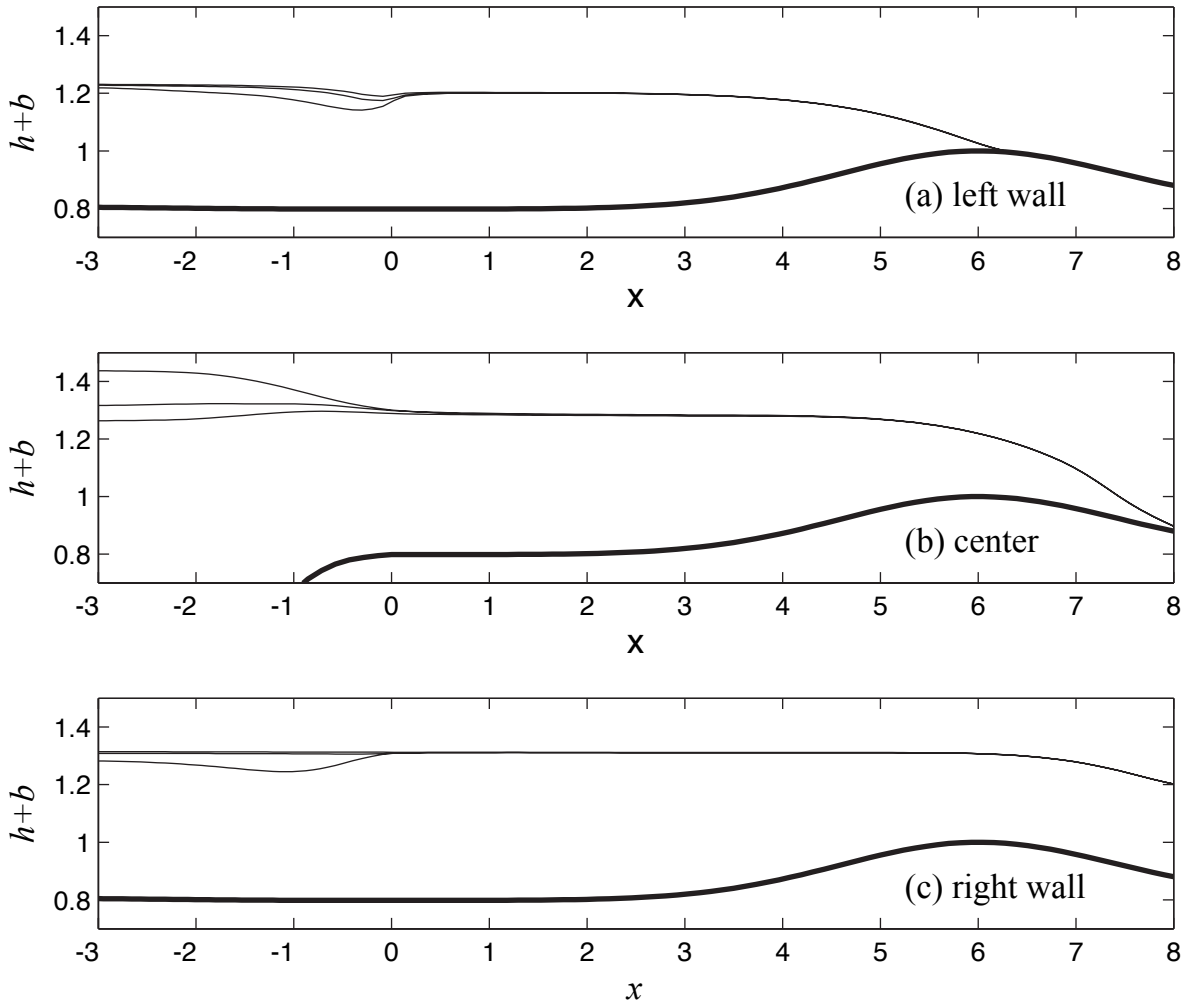
h+b
1.4
1.2
1
0.8
-3
-2
-1
0
1
2
3
4
5
6
7
8
x
(a) left wall
h+b
(b) center
x
h+b
(c) right wall
x

Figure 2.13.5

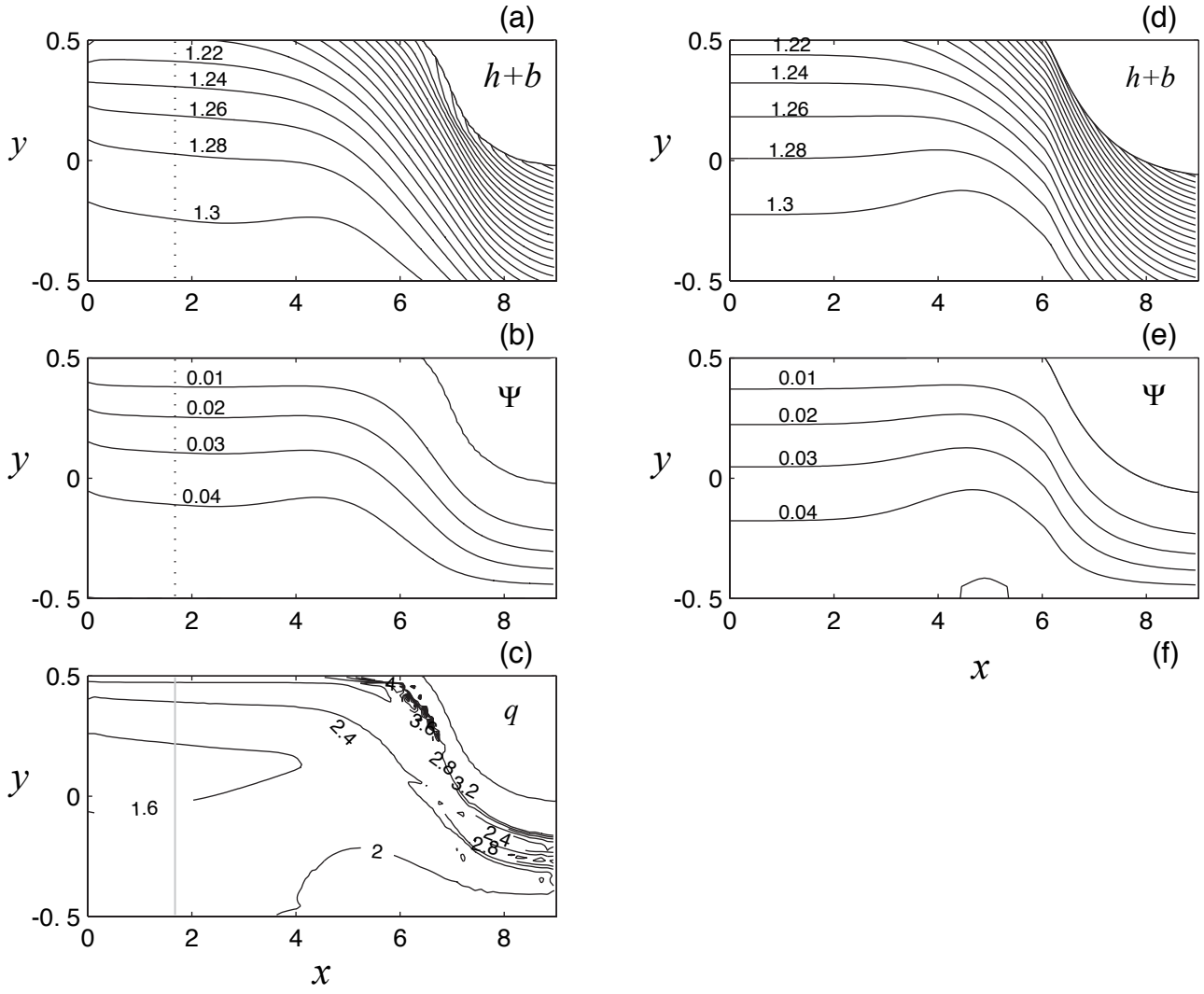
(a)
h+b
1.22
1.24
1.26
1.28
1.3
(b)
Ψ
0.01
0.02
0.03
0.04
(c)
q
1.6
2
2.4
2.8
3.2
(d)
h+b
1.22
1.24
1.26
1.28
1.3
(e)
Ψ
0.01
0.02
0.03
0.04
(f)
y
x
0.5
0
-0.5
0
2
4
6
8

Figure 2.13.6

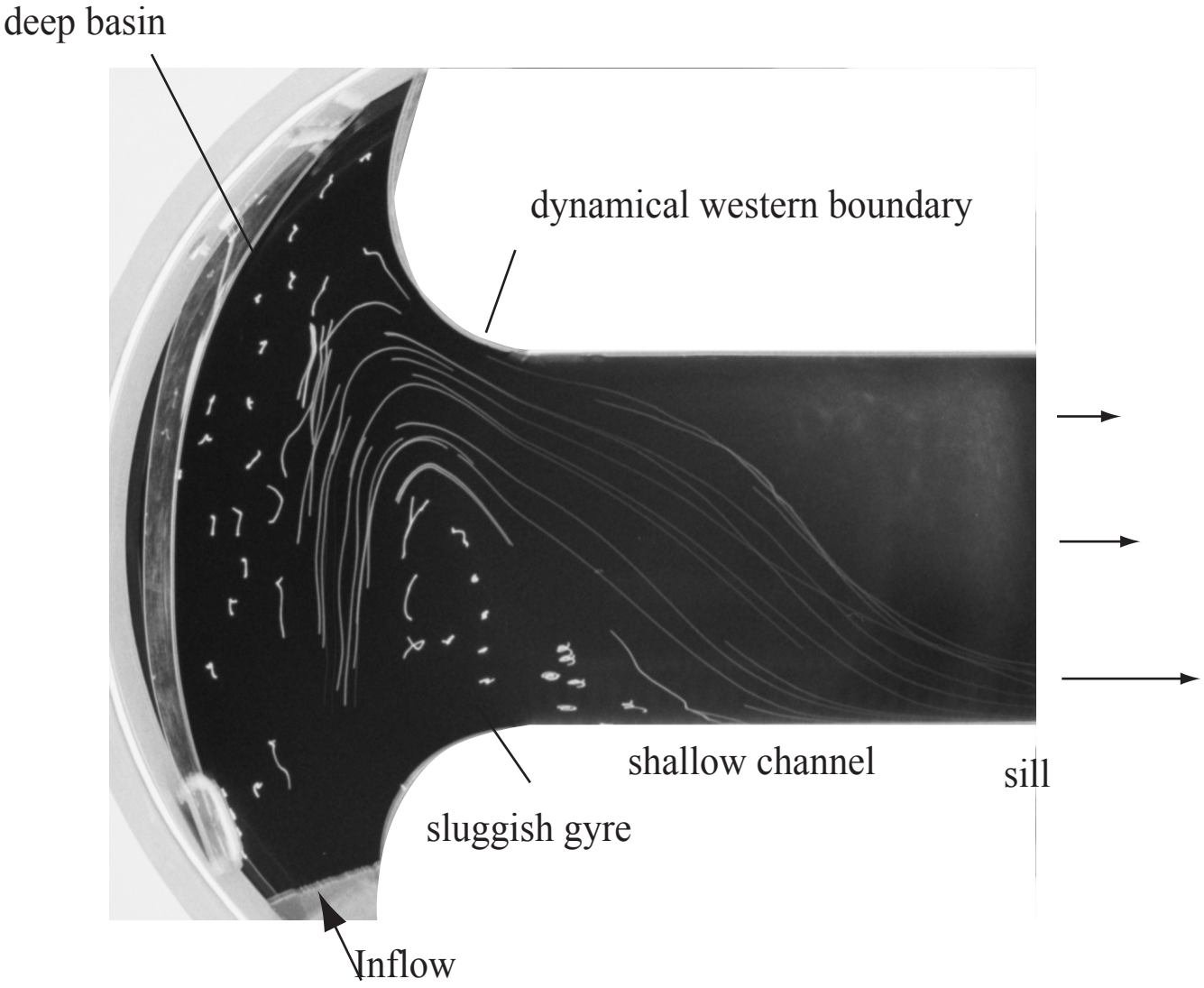

(a)

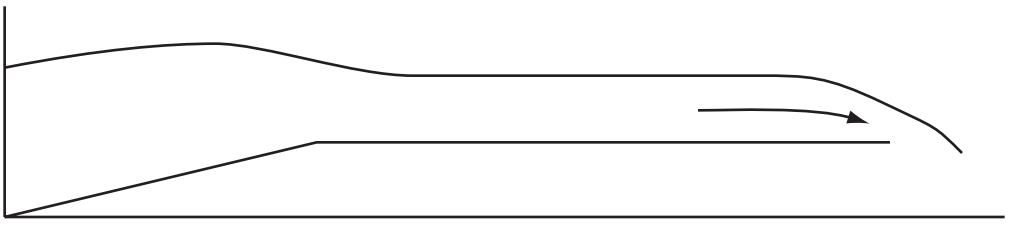

(b)

Figure2.13.7